American Genetic Association

Journal of Heredity, 2021, 1–10
doi:10.1093/jhered/esab001
Original Article
Advance Access publication January 13, 2021

OXFORD

Original Article

Extensive Linkage and Genetic Coupling of Song and Preference Loci Underlying Rapid Speciation in *Laupala* Crickets

Mingzi Xu and Kerry L. Shaw

From the Department of Neurobiology and Behavior, Cornell University, Ithaca, NY 14853 (Xu and Shaw).

Address correspondence to M. Xu at the address above, or e-mail: xu000574@umn.edu.

Received August 15, 2020; First decision December 19, 2020; Accepted January 11, 2021.

Corresponding Editor: Scott Hodges

Abstract

In nature, closely related species commonly display divergent mating behaviors, suggesting a central role for such traits in the origin of species. Elucidating the genetic basis of divergence in these traits is necessary to understand the evolutionary process leading to reproductive barriers and speciation. The rapidly speciating Hawaiian crickets of the genus *Laupala* provides an ideal system for dissecting the genetic basis of mating behavior divergence. In *Laupala*, closely related species differ markedly in male song pulse rate and female preference for pulse rate. These behaviors play an important role in determining mating patterns. Previous studies identified a genetic architecture consisting of numerous small to moderate effect loci causing interspecific differences in pulse rate and preference, including colocalizing pulse rate and preference QTL on linkage group one (LG1). To further interrogate these QTL, we conduct a fine mapping study using high-density SNP linkage maps. With improved statistical power and map resolution, we provide robust evidence for genetic coupling between song and preference, along with two additional pulse rate QTL on LG1, revealing a more resolved picture of the genetic architecture underlying mating behavior divergence. Our sequence-based genetic map, along with dramatically narrowed QTL confidence intervals, allowed us to annotate genes within the QTL regions and identify several exciting candidate genes underlying variation in pulse rate and preference divergence. Such knowledge suggests potential molecular mechanisms underlying the evolution of behavioral barriers.

Subject Area: Quantitative genetics
Key words: reproductive isolation, genetic architecture, genetic coupling, acoustic signal, quantitative genetics, candidate gene

Divergent mating signals and signal preferences create one of the most potent barriers to gene flow during early stages of speciation (Panhuis et al. 2001; Ritchie 2007; Uy et al. 2018). Knowledge of the genetics of such behavioral barriers can grant us insight into genetic processes leading to speciation. Yet the genetic basis of divergent mating phenotypes remains a poorly understood component of the evolutionary process (Wilkinson et al. 2015).

The unsolved problem is 3-fold. First, while signals and preferences diverge among lineages, they must coevolve within a lineage to maintain mate recognition and compatibility (Fowler-Finn and Rodríguez 2016). What genetic mechanism facilitates coevolution between male signals and female preferences? Although both linkage disequilibrium between signal and preference alleles (Fisher 1930; Lande 1984) and genetic coupling, that is, a single pleiotropic gene

or tightly linked genes regulating both traits (Alexander 1962; Butlin and Ritchie 1989; Singh and Shaw 2012) can mediate signal-preference coevolution, we have very limited insight into which mechanism is more likely. A second unanswered question concerns the genetic architecture underlying the evolution of behavioral barriers (Templeton 1981). As signals and preferences are commonly quantitative traits thought to be under stabilizing selection (Henry et al. 2002; Saldamando et al. 2005; Limousin et al. 2012; Oh et al. 2012; Bay et al. 2017; Merrill et al. 2019), variation in these traits likely involves a genetic architecture consisting of many genes of small effect (type I). In contrast, a genetic architecture consisting of few loci of large effect (type II) has been identified in some systems (Kronforst et al. 2006; Gould et al. 2010; Ding et al. 2016). This discrepancy suggests a potentially biased and incomplete picture due to challenges in detecting genetic factors of small effect. Lastly, while a few cases are known (e.g., Fang et al. 2002; Ding et al. 2016), causal genes underlying divergent mating signals, and especially those underlying divergent preferences, remain elusive.

The rapidly radiating Hawaiian cricket genus *Laupala* has been proven a powerful system for dissecting the genetic basis underlying divergent mating behavior. Male *Laupala* mating songs have species-typical pulse rates that attract females. In response, female *Laupala* express acoustic preference for conspecific pulse rates through phonotaxis (i.e., orienting and walking toward the preferred sound source; Shaw 2000; Shaw and Herlihy 2000; Mendelson and Shaw 2002; Oh and Shaw 2013). Species of *Laupala* are morphologically and ecologically similar (Otte 1994; Xu and Shaw 2020), while conspicuous divergence in mating songs and preferences suggests sexual selection as a primary mechanism driving rapid speciation (Mendelson and Shaw 2005).

Prior work on the genetics of divergent acoustic behavior in *Laupala* supports an intriguing type I genetic architecture for both signal and preference traits with evidence for colocalized trait and preference genes. In interspecific studies of the fast singing *Laupala kohalensis* and the slow singing *Laupala paranigra*, genome-wide quantitative genetic analyses revealed a polygenic genetic architecture consisting of small- to moderate-effect quantitative trait loci (QTL) distributed across the genome (Shaw et al. 2007; Ellison and Shaw 2013). Additionally, genome-wide mapping studies found evidence for colocalized song and preference QTL on linkage group one (LG1) (Shaw and Lesnick 2009; Wiley et al. 2012). Further work using a fine mapping approach on LG5 found an additional pair of colocalizing pulse rate and preference loci as close as 0.06 cM apart (Xu and Shaw 2019a).

In this study, using the *L. kohalensis* and *L. paranigra* species pair and recently published *Laupala* genome resources (Blankers, Oh, Bombarely et al. 2018; Blankers, Oh, and Shaw 2018; Xu and Shaw 2019), we isolate the previously identified pulse rate QTL on LG1 in near-isogenic lines (NILs) and interrogate this linkage group through fine mapping to accomplish three goals. First, we aim to refine location and confidence interval (CI) estimates of pulse rate and preference QTL on LG1. Previous results on LG1 were limited by low marker density and statistical power, resulting in wide CIs and low resolution location estimates of the pulse rate and preference QTL (Shaw et al. 2007; Shaw and Lesnick 2009). Here, we construct high-density linkage maps using single nucleotide polymorphisms (SNP) to improve both map resolution and coverage. Second, we test for additional pulse rate and/or preference QTL on LG1. A recent high resolution mapping study on LG5 detected several additional small-effect pulse rate loci (Xu and Shaw 2019), illustrating benefits of a fine mapping approach utilizing NILs. Finally, we annotate QTL regions on LG1 to identify candidate genes underlying pulse rate and preference divergence. Previous mapping efforts on LG1 relied on AFLP markers, providing no means to identify the causal genes.

Materials and Methods

Breeding Design

Using a two-stage breeding design, we first isolated the focal QTL (QTL1) in a near isogenic line (NIL1D.2; for details see Supplementary Material), then generated NIL-F_2 mapping populations (Figure 1). NIL1D.2 was created by hybridizing a *L. kohalensis* female with a *L. paranigra* male, both from isofemale lines, followed by backcrossing to *L. kohalensis* for four generations selecting only offspring carrying an *L. paranigra* AFLP marker linked to the major *L. paranigra* QTL1 allele (Shaw et al. 2007). Fourth generation backcross individuals were intercrossed to generate the NIL1D.2, where the *L. paranigra* genotype at QTL1 was maintained through intercrossing for nine generations. In the second step, we created five F_2 mapping families (denoted 1D.2.5, 1D.2.6, 1D.2.8, 1D.2.9, and 1D.2.13, Supplementary Table S1) by backcrossing NIL males with recurrent line *L. kohalensis* females and intercrossing their offspring. Parental *L. kohalensis* and NIL lines were maintained alongside mapping populations.

Crickets were reared individually in 120 mL specimen cups with moist tissue and ad libitum Organix organic chicken and brown rice dry cat food (Castor & Pollux Natural Petworks, Clackamas, OR) in a rearing room at 20.0 °C and light cycle at 12L:12D.

Male Song Phenotyping

We recorded male songs from parental lines and NIL-F_2 families with an Olympus WS-852 digital stereo recorder (Olympus Imaging Corp., Tokyo, Japan) during daylight hours at controlled temperatures (20.2 ± 0.01 °C, mean ± SE, n = 238). Digital sound files were analyzed using RavenPro 1.4 (www.birds.cornell.edu/raven). Pulse period was measured as the time differential between the beginning of two consecutive pulses. Mean pulse rate (pulses per second, pps) was calculated by taking the inverse of mean pulse period from five independent pulse period measurements per male.

Female Preference Phenotyping

Peak pulse rate preference was estimated from phonotaxis trials for each female from all NIL-F_2 families in a sound isolation booth (RS-243, ETS-Lindgren, Wood Dale, IL) at c. 20 °C (20.1 ± 0.01 °C, mean ± SE, n = 468). Phonotaxis and playback design has been described previously (Xu and Shaw 2019). Briefly, each trial involved a 5-min pretrial and 10-min testing period. Two simulated songs were broadcast simultaneously, one from each of two speakers placed at opposite ends of a 90 cm phonotaxis tube. During the pretrial period, the focal female was confined to the central portion of the tube. To commence the testing period, the central portion was opened via rotatable doors to the distal ends of the phonotaxis tube, allowing the female to approach one or the other speaker. If a female entered the preference zone defined as the distal 10 cm at each end of the tube, we scored a preference for the song pulse rate from that speaker.

All females were initially tested in four trials where pulse rates of the two songs were 3.0 versus 3.5 pps, 3.1 versus 3.6 pps, 3.2 versus 3.7 pps, and 3.3 versus 3.8 pps. Other song parameters were identical among all simulated songs (pulse duration = 40 ms, carrier frequency = 5 kHz) and were characteristic of both species (Shaw 2000). Songs were randomized by speaker for each trial. If female

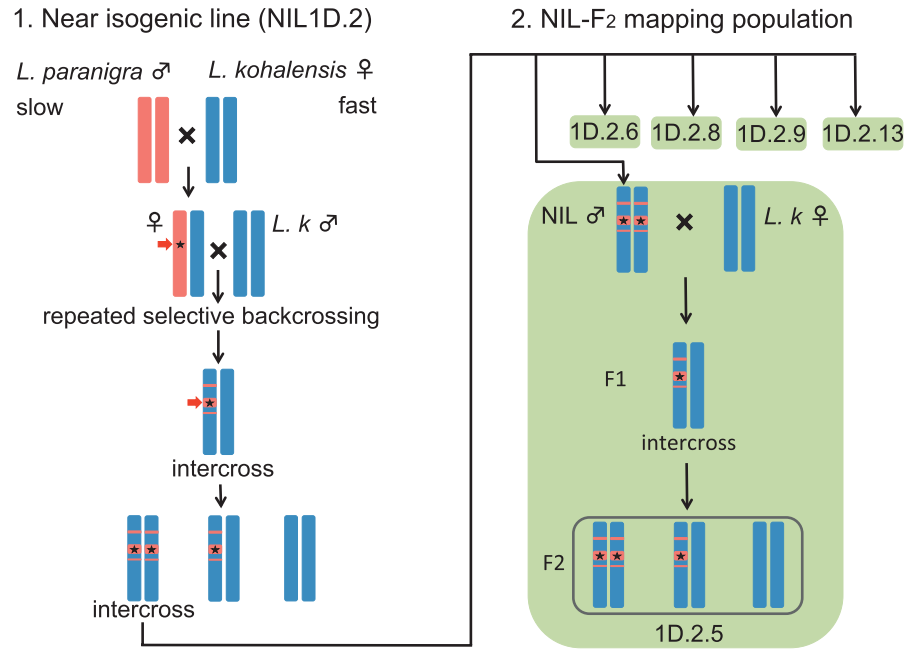

Figure 1. A two-step breeding design for QTL fine mapping of variation in male song pulse rate and female peak preference for pulse rate between *L. paranigra* (slow singer) and *L. kohalensis* (fast singer) on LG1 (represented by red and blue bars). In step 1, near isogenic lines (NILs) were created through four generations of marker assisted backcrossing (indicated by red arrow) selecting for individuals carrying the *L. paranigra* allele at the genetic marker linked to QTL1 in Shaw et al. (2007) (indicated by the black star) and one generation of intercrossing. In step 2, NIL males were backcrossed to *L. kohalensis* females to generate five independent segregating F_2 mapping populations. Only the detailed process to obtain 1D.2.5 is shown; the process is the same for all other families. See online version for full colors.

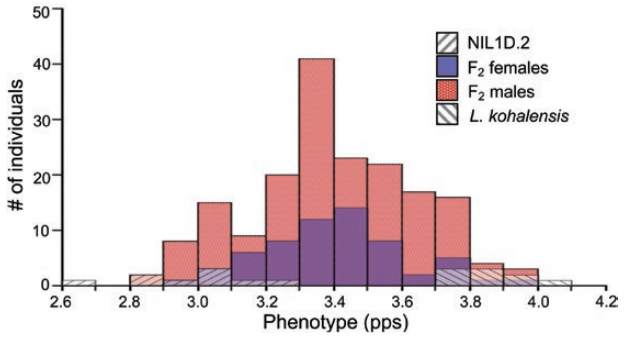

Figure 2. Phenotypic distributions of parental *L. kohalensis,* near isogenic line 1D.2 (NIL1D.2), and males and females from all NIL-F_2 intercross families. The histograms are overlaid. Phenotypic values are measured in the unit of pps. See online version for full colors.

response switched from faster pulse rate at the lower end to slower pulse rate at the higher end of the trial range, peak preference was estimated on the basis of these four trials as the midpoint of the switch from faster to slower pulse rates (for an example of the estimation see Figure 2b in Xu and Shaw 2019a). If the female showed consistent response to slower or faster pulse rate in the initial four trials, she was further tested in up to three trials at either slower (2.7 vs. 3.2 pps, 2.8 vs. 3.3 pps, and 2.9 vs. 3.4 pps) or faster (3.4 vs. 3.9 pps and 3.5 vs. 4.0 pps, 3.6 vs. 4.1 pps) end of the pulse rate range, depending on the direction of her response in the initial trials. We repeated each trial up to six times for females who failed to respond in a given trial. On any given day, females were tested in no more than two trials, with at least 2 h between the trials. In cases where a female consistently showed preference for faster or slower pulse rates in all seven trials, we estimated the peak preference at the most conservative value (i.e., the midpoint in the next extreme trial, assuming the female would show a switch in her preference).

Genotyping

We obtained SNP-based genotypes from NIL-F_2 families using Genotyping-by-Sequencing (Elshire et al. 2011) on the Illumina HiSeq2000 platform at the Genomic Diversity Facility at Cornell University (see Supplementary Material for details). Sequencing reads were demultiplexed using fastq-multx v.1.3.2 (Aronesty 2011). We trimmed Illumina adaptors and nucleotides with base call Phred scrore <30 at the ends of the reads and filtered out reads less than 50 bases long with fastq-mcf v.1.04.636 (Aronesty 2011). Processed reads were aligned to the *L. kohalensis* reference genome (NCBI accession ASM231320v1, Blankers, Oh, Bombarely et al. 2018) using Bowtie2 v.2.2.6 (Langmead and Salzberg 2012) with default parameter settings. We pooled all F_2 families to call SNP variants allowing for a maximum of two mismatches per mapped read using FreeBayes v.0.9.12-2-ga830efd (Garrison and Marth 2012). The resulting SNP markers were filtered using VCFtools 0.1.15 (Danecek et al. 2011) and vcffilter in vcflib v.1.0.0 (Garrison 2012). We retained bi-allelic SNP markers that fulfill the following criteria: 1) <20% missing data, 2) minor allele frequency ≥2.5%, 3) genotype depth ≥5, 4) Phred scaled variant quality ≥30, and 5) strand balance probability for reference and alternative alleles >0.0001. Because parental NIL and *L. kohalensis* individuals were lost, F_2 genotypes were called using the *L. kohalensis* genome reference as the *L. kohalensis* parent; the alternative allele was assigned to the NIL parent.

Linkage Mapping

We constructed linkage maps of autosomal linkage groups using genotypes at SNP markers from F_2 individuals in Joinmap 4

(Van Ooijen 2006). Markers deviating from a segregation ratio of 1:2:1 (Benjamini–Hochberg adjusted $P < 0.05$) and/or whose mean depth of coverage <20 were excluded from linkage mapping. Two types of linkage maps were constructed. First, we constructed individual family linkage maps of the two largest families, 1D.2.5 and 1D.2.8. Other families were too small to estimate individual family linkage maps. Maps were estimated using the regression algorithm (for details see Supplementary Material) and thinned by retaining one marker per scaffold. Second, we integrated LG1 from the two families, retaining only markers whose orders were consistent in the two families and had nearest neighbor fit < 10 cM (see Supplementary Material for explanation) on the integrated map. This mapping strategy resulted in maximizing map coverage and density for individual-family-maps and highly confident marker order for the integrated map. We did not integrate maps of other LGs because the two families shared few markers.

QTL Mapping

Individuals with scored phenotypes and <25% missing genotypes were used for QTL mapping. We performed standard interval mapping (SIM) and multiple QTL mapping (MQM) for males and females separately in R/qtl v.1.39–5 (Broman et al. 2003). QTL mapping was first conducted in 1D.2.5 and 1D.2.8 separately on their respective maps, and then using data from all families on the integrated map. For the latter, we tested for family effect on phenotypes and subsequently included family as a covariate in SIM and MQM for both pulse rate and preference. We estimated effect sizes and 1.5-LOD CIs of significant QTL from the final MQM models. For details of SIM, MQM, and LOD threshold calculations see Supplementary Material.

Gene Prediction and Functional Annotation

To identify candidate genes for interspecific variation in pulse rate and preference on LG1, we annotated scaffolds within and immediately flanking the 1.5-LOD CIs of all pulse rate and preference QTL from both SIM and MQM on the integrated map. We also annotated scaffolds unique to individual family maps (1D.2.5 and 1D.2.8) that were not present in the integrated map but coincided with the CIs of significant QTL (Supplementary Figure S1).

We conducted gene prediction and structural annotation using the Maker pipeline (Cantarel et al. 2008). We used SNAP (Korf 2004) and Augustus-3.2.3 (Stanke and Morgenstern 2005) for ab initio gene prediction and conducted alignment-based annotation with available RNA, EST, and protein evidence (Danley et al. 2007; Bailey et al. 2013; Zeng et al. 2013; Berdan et al. 2016; Xu and Shaw 2019). Detailed information on gene prediction can be found in the Supplementary Material.

We then functionally annotated the predicted genes by blasting their sequences against the Animalia subset of the NCBI nonredundant protein and the UniProt databases (Apweiler et al. 2004) using an E-value cutoff of 1E-4. For adjacent genes with the same annotation, we manually inspected the annotation by re-blasting the joined region and subsequently refined gene identity and boundary annotation using protein2genome alignment between the *Laupala* sequence and the protein sequence of the top blast hit in Exonerate 2.2.0 (Slater and Birney 2005). We annotated gene ontologies (GO; Ashburner et al. 2000) using the UniProt database. To identify any remaining predicted genes lacking an annotation, we reran blast for these sequences using a relaxed E-value cutoff of 100.

Results

Parental and NIL-F_2 Phenotypes

Males from the parental *L. kohalensis* line sang with faster pulse rates (n = 9, 3.87 ± 0.03 pps, mean ± SE, Figure 2) and males from NIL1D.2 sang with slower pulse rates (n = 9, 2.99 ± 0.06 pps). The mean of the F_2 mapping population was intermediate between the parents (n = 241, 3.39 ± 0.01 pps) and with variation overlapping the parental phenotypes for both pulse rate and preference (Figure 2).

Linkage Mapping

In 1D.2.5 and 1D.2.8 linkage maps, marker numbers and density were the highest on LG1, with median marker intervals of 0.67 and 1.73 cM, respectively (Supplementary Tables S2–S3). The order of shared markers on LG1 was highly consistent between the two families (Supplementary Figure S1). The integrated map contained 43 markers (Supplementary Figure S1) with highly consistent order and a median marker interval of 2.33 cM (Supplementary Table S4).

Multiple Linked Pulse Rate QTL on LG1

In SIM using combined data from all families on the integrated map, we localized a pulse rate QTL at 63 cM on LG1 (Table 1, Figure 3), which was consistent with location estimates based on common markers from individual-family mapping in both 1D.2.5 and 1D.2.8 (Supplementary Table S5; Supplementary Figures S2 and S3). The CI of this pulse rate QTL spanned 0.6 cM and included two scaffolds (S000494 and S004771). The homologous regions on the 1D.2.5 and 1D.2.8 maps included two additional scaffolds (S000949 and S004205).

In MQM, we identified three additional linked pulse rate QTL (QTL1.1m, QTL1.3m, and QTL1.4m) in addition to that identified in SIM above (QTL1.2m, Table 1, Figure 4). The phenotypic effect of a single allele at each of the four QTL was primarily additive, ranging from approximately 2–6% of the species difference. In all cases, *L. kohalensis* alleles increased, whereas *L. paranigra* alleles decreased, the pulse rate in hybrids (Table 1, Figure 4). Together, their allelic effects accounted for 14.3% of the species difference in pulse rate and 76.9% of F_2 phenotypic variance.

Refined Localization of Preference QTL on LG1

In SIM using data from combined families on the integrated map, we localized a preference QTL at 60.1 cM (Table 1, Figure 3). The CI spanned 11.7 cM and included eight scaffolds (Figure 3, scaffolds in black). This preference QTL had an additive effect of 0.27 ± 0.04 pps, explaining 9.0% of species difference and 52.7% of F_2 phenotypic variance. Within the CI of the preference QTL are two additional peaks at 62.8 and 69.6 cM, just 0.31 and 0.05 LOD lower, respectively, than that of the peak at 60.1 cM (Figure 3), although they were not recognized as independent QTL. In MQM, the preference QTL was estimated at one of these other locations (69.6 cM, QTL1.5f, Table 1), with the MQM LOD profile suggesting an additional, but nonsignificant, peak at 60.4 cM (the location of the SIM preference estimate, at 0.21 LOD lower than the MQM recognized QTL at 69.6 cM, Figure 4).

Colocalization of Pulse Rate and Preference QTL

In SIM, the peaks of pulse rate and preference QTL were 2.9 cM apart. The CI of the preference QTL completely included that of the pulse rate QTL (Table 1, Figure 3). Consistent with SIM, MQM showed that the

Table 1. Results from standard interval mapping and multiple QTL mapping of variation in male song pulse rate and female peak preference for pulse rate on the integrated map using the combined data from all F_2 families

Trait	Standard interval mapping			Multiple QTL mapping			QTL effect size-additive (pps ± SE)	% Species difference explained	% F_2 variance explained
	QTL location (cM)	LOD score (threshold)	1.5-LOD CI (cM)	QTL name	QTL location (cM)	LOD score (threshold)	1.5-LOD CI (cM)			
Pulse rate	–	–	–	QTL1.1m	56.60	9.59 (2.60)	55.40–58.80	0.14 ± 0.02	4.65	5.67
Pulse rate	63.00	41.57 (2.74)	62.60–63.25	QTL1.2m	63.20	12.61 (2.60)	63.00–64.80	0.16 ± 0.02	5.32	66.92
Pulse rate	–	–	–	QTL1.3m	97.20	3.09 (2.60)	77.80–107.00	0.06 ± 0.02	1.99	1.66
Pulse rate	–	–	–	QTL1.4m	124.48	4.79 (2.60)	122.40–143.61	0.07 ± 0.02	2.33	2.63
Preference	60.11	7.87 (3.03)	58.20–69.94	QTL1.5f	69.60	8.13 (3.04)	58.40–69.94	0.27 ± 0.04	8.97	52.69

CI of the significant preference QTL (QTL1.5f) completely included that of QTL1.2m, the same pulse rate QTL identified by SIM (Figure 4).

As stated above, the phenotypic effect of the colocalizing pulse rate and preference QTL were both positive, primarily additive, and moderate in size (5–9% of the species difference). In addition, males and females showed similar phenotypic distributions at the markers with the highest LOD score: individuals with the *L. paranigra*-origin (AA), the heterozygous, and the *L. kohalensis*-origin (BB) genotype showed lower (male: 3.07 ± 0.03 pps, mean ± SE, female: 3.03 ± 0.08 pps, Figure 3), intermediate (male: 3.36 ± 0.01 pps, female: 3.30 ± 0.03 pps), and higher phenotypic values (male: 3.68 ± 0.02 pps, female: 3.56 ± 0.04 pps), respectively.

Annotation of the QTL Regions

We annotated a total of 52 scaffolds within the cumulative CIs of pulse rate and preference QTL on LG1 (Supplementary Figure S1) arising from individual family and integrated map analyses. After filtering out transposable element genes, Maker predicted 245 genes on 39 scaffolds (5 scaffolds contained only transposable element genes and the remainder contained no predicted genes). Among the 245 genes, 189 had significant blast hits to the protein databases, of which 152 had associated GO terms (Supplementary Table S6). Repeating the blast at a relaxed E cutoff of 100 for the remaining 56 genes left 11 un-annotated (Supplementary Table S6). The annotated gene functions include regulation of cell cycle, gene expression, development, cellular transportation, biosynthesis, metabolic processes, signal transduction, neural functioning and modulation, and response to stress (Supplementary Table S6).

Within the CI of both QTL1.2m and QTL1.5f, dynein light chain 90F (*Dlc90F*, #39 in Supplementary Table S6) and synaptosomal-associated protein 25 (*Snap25*, #47 in Supplementary Table S6), located on scaffold S000494, the scaffold with the highest LOD score for QTL1.2m, have functions pertaining to connectivity of neural circuits, specifically, neurite development and synaptic transmission. Another gene within the CI of QTL1.5f on scaffold S003059, protein phosphatase 1 regulatory subunit 9A (*Ppp1r9a*, also known as neurabin-1, # 223 in Supplementary Table S6), also functions in neuron projection development. We also identified two genes relevant for central pattern generator or pacemaker functioning: innexin 2 (*Inx2*, #78 in Supplementary Table S6) located on scaffold S008276 within in the CI of QTL1.5f and anoctamin 1 (*Ano1*, also known as *TMEM16A*, #116) on scaffold S002553 within the CI of QTL1.3m. Among the annotated genes within the CI of QTL1.3m on scaffold S004073 was also a *Laupala* homolog of the *Drosophila Camta* gene (#119) connected to song rhythm regulation in *Drosophila* (Yokokura et al. 1995; Gleason and Ritchie 2004).

Discussion

Divergent behaviors, especially those involved in sexual communication, often play a central role in establishing barriers to gene exchange during early stages of speciation (Coyne and Orr 2004; Ritchie 2007). The genetic basis underlying behavioral barriers is thus crucial to explaining the process of speciation yet how these barriers evolve remains poorly understood on many fronts (Shaw and Mullen 2011; Wilkinson et al. 2015), including the underlying genetic architecture, the coevolution of sex-limited traits, and the genes involved. Current evidence on the evolution and genetics of acoustic communication supports a type I genetic architecture involving many genes of relatively small effect contributing to differences between

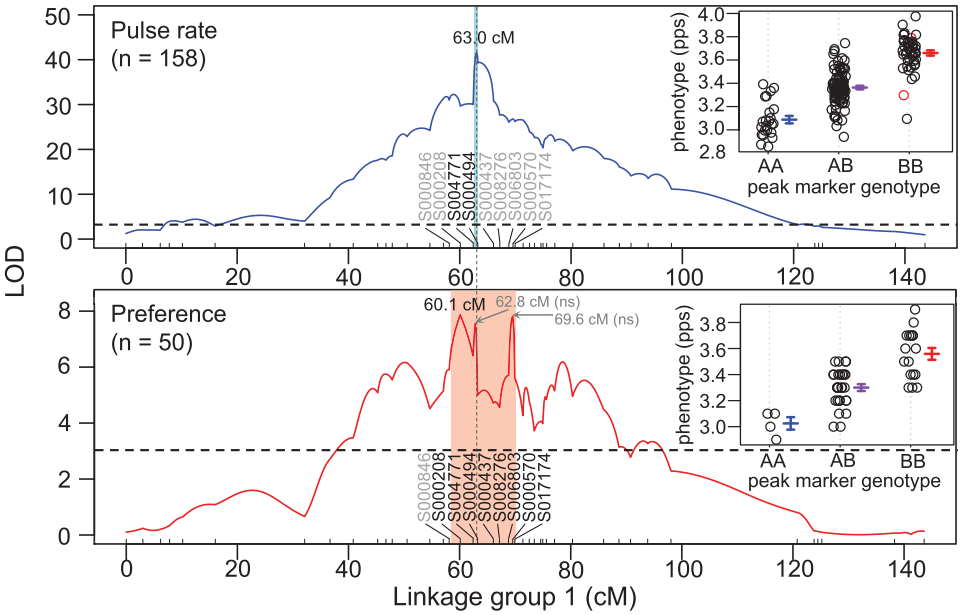

Figure 3. LOD profiles and phenotypic effects of alleles at the markers with the highest LOD score from standard interval mapping of interspecific variation in pulse rate and preference using the combined data from all F_2 families on the integrated map. The red and blue shaded areas indicate 1.5-LOD CIs for preference and pulse rate QTL, respectively. Markers within and flanking the CIs of QTL are labeled in black and grey, respectively. The scatter plots show individual phenotypes for three genotypes at the marker with the highest LOD score for preference and pulse rate; the middle horizontal lines are means and the whiskers are standard errors. Black and red circles in the scatter plots are individuals with actual and simulated genotypes. The horizontal dotted lines indicate significance thresholds. Additional nonsignificant (ns) peaks within the CI of preference QTL were labeled by grey arrows and their locations. The vertical dotted line indicates the location of the third highest LOD peak within the CI of the preference QTL, corresponding with the location of pulse rate QTL. See online version for full colors.

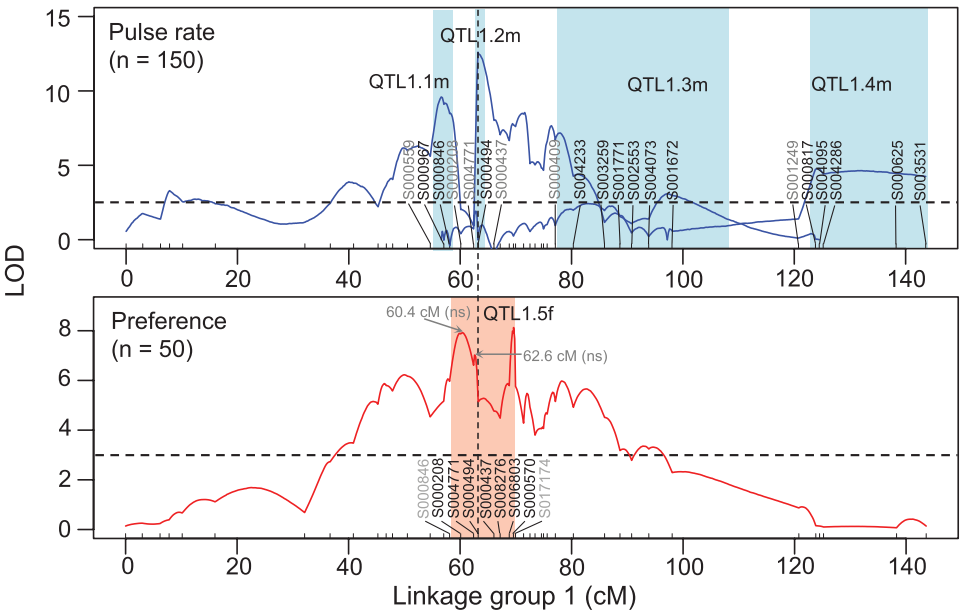

Figure 4. LOD profiles from multiple QTL mapping of interspecific variation in pulse rate and preference using the combined data from all F_2 families on the integrated map. The red and blue shaded areas indicate 1.5-LOD CIs for significant QTL. Markers within and flanking the CIs of QTL are labeled in black and grey, respectively. The horizontal dotted lines indicate significance thresholds. The vertical dotted line indicates the location of QTL1.2m. Additional nonsignificant (ns) peaks within the CI of preference QTL were labeled by grey arrows and their locations. See online version for full colors.

Laupala species and an emerging pattern of genetic coupling (tight physical linkage or pleiotropy) among QTL involved in male and female mating behaviors (Shaw et al. 2007; Shaw and Lesnick 2009; Blankers et al. 2019; Xu and Shaw 2019). Here, we conduct a fine-scale dissection of LG1 using a high-resolution linkage map and selective introgression of song and preference QTL. We also provide annotation of QTL regions to identify candidate genes for interspecific variation in pulse rate and pulse rate preference.

Our results add strong evidence and more detail to the picture of a type I genetic architecture underlying song and preference variation

between *Laupala* species. With increased statistical power and map resolution on LG1, we identified four linked pulse rate QTL on LG1 (Figure 4, Table 1), doubling that previously known. Based on map position and phenotypic effect sizes, the present results have likely resolved each of the two previously identified pulse rate QTL (Shaw et al. 2007) into two. The largest QTL on this linkage group (QTL1; Shaw et al. 2007) likely traces to closely linked QTL1.1m and QTL1.2m in the present study.

We also find significant evidence from SIM for one preference QTL at 60.1 cM (Figure 3, Table 1), corroborating a previous estimate from an independent iteration of the same species cross (Shaw and Lesnick 2009). Two additional peaks in the LOD profile (at 62.8 and 69.6 cM) are suggested by the SIM within the CI with very small LOD differentials from the significant QTL (at 60.1 cM), although they lack statistical significance as independent QTL, likely due to limited sample sizes and nonindependent segregation (i.e., tight linkage; Figure 3). Indeed, the location of the significant preference QTL moved from 60.1 cM in SIM to one of these other positions (69.6 cM) in MQM, with the SIM peak location (60.1 cM) showing only a slightly lower LOD in the MQM profile (Figures 3 and 4). We hypothesize that like pulse rate, two or more tightly linked preference QTL lie in this region on LG1, a test of which awaits future study.

These patterns, together with those found on other linkage groups (Shaw et al. 2007; Wiley and Shaw 2010; Blankers et al. 2019; Xu and Shaw 2019), suggest that evolution of male pulse rate and preference for pulse rate diverged by an accumulation of small steps in *Laupala*, as opposed to single switch type of change observed in some other rapidly evolving sexual traits (Reed et al. 2011; Pascoal et al. 2014). We note that a type I genetic architecture is often thought to be associated with a slow and gradual evolutionary process, yet acoustic behavior and their consequences for reproductive barriers have evolved rapidly in *Laupala* (Mendelson and Shaw 2005). Our findings suggest that close linkage (or pleiotropy) between pulse rate and preference loci as we discuss below may have contributed to the rapid divergence of mating behaviors in spite of a type I genetic architecture.

Adding strength to previous findings, we localized overlapping pulse rate and preference QTL (QTL1.2m and QTL1.5f) on LG1 (Figures 3 and 4, Table 1) at locations coincident with previous estimates (Shaw et al. 2007; Shaw and Lesnick 2009). Further, the location of QTL1.2m is corroborated by both mapping families (1D.2.5 and 1D.2.8). Remarkably, the estimated peak locations for the pulse rate and preference QTL were just 2.9 cM apart in SIM (Table 1) and the CI of the pulse rate QTL is completely included within that of the preference QTL in both SIM and MQM (Figures 3 and 4). Intriguingly, one of the additional (although nonsignificant) preference peaks corresponds exactly with the estimated peak location of the pulse rate QTL (Figures 3 and 4, vertical dotted line). Importantly, as required for signal-preference coevolution, the phenotypic effects of the colocalizing pulse rate and preference QTL were in the same direction.

These results provided robust evidence for genetic coupling underlying signal-preference coevolution. Although linkage disequilibrium between unlinked genes has been presumed as the primary mechanism promoting signal-preference coevolution (Lande 1981; Roff and Fairbairn 2014), linkage disequilibrium can be easily eroded by recombination. It is thus open to question how effective this mechanism is in establishing reproductive barriers during early stages of speciation in the presence of gene flow. In comparison, genetic coupling provides an effective mechanism to counter the homogenizing effect of gene flow during early stages of speciation and facilitate the establishment and maintenance of premating isolation (Kopp et al. 2018). Colocalizing pulse rate and preference QTL on both LG1 herein and on LG5 (Xu and Shaw 2019) from *Laupala* crickets is among a group of recently emerged findings (Kronforst et al. 2006; Bay et al. 2017; Brand et al. 2019; Merrill et al. 2019) that demonstrate genetic coupling may be more widespread in nature than we have previously thought and may have played an important role in rapid speciation.

Our fine mapping strategy has substantially increased map resolution and mapping precision. Average marker spacing on LG1 has improved from 5 to 8 cM in previous work (Shaw et al. 2007) to 0.7 and 1.7 cM in 1D.2.5 and 1D.2.8, respectively (Supplementary Table S3); likewise, distance between the focal QTL and the closest marker has decreased from 1.2 cM (Shaw et al. 2007; Shaw and Lesnick 2009) to 0.05 cM for pulse rate and 0.03 cM for preference in MQM (Table 1). In addition, CIs of the colocalizing QTL have decreased from 13 and 26 cM (Shaw and Lesnick 2009) to 0.6 and 11.7 cM for pulse rate and preference, respectively (Table 1). These improvements, coupled with knowledge of the genome (Blankers et al. 2018), enabled our annotation of the relevant genomic regions and identification of candidate genes underlying pulse rate and preference variation.

Mechanistically, the regular pulses of cricket songs are due to patterned motor output driven by neural circuits called central pattern generators (Chagnaud and Bass 2014; Katz 2016; Schöneich and Hedwig 2017). In female crickets, pulse rate preference is realized through a neural circuit wherein direct and delayed line inputs to a coincidence detector neuron are offset in time equivalent to conspecific pulse period through post-inhibitory rebound (Schöneich et al. 2015). Therefore, phenotypic evolution in both song pulse rate and preference can be genetically enabled by genes that regulate either the excitatory properties of neurons or the wiring of relevant neural circuits (Harris-Warrick 2010; Katz 2016). The former case includes genes pertaining to number, type, or functioning of ion channels (Harris-Warrick 2010) and the latter includes genes that regulate axonal pathfinding, presynaptic cell surface proteins, neurotransmitter synthesis and release, and neuronal identity transcription factors (Tosches 2017).

Within this mechanistic framework, our annotation revealed numerous candidate genes with relevant functions. On scaffold S000494, the scaffold with the highest LOD score for QTL1.2m and within the CI of QTL1.5f, two genes showed functions relevant for rewiring of neural circuits. *Dlc90F* (#39 in Supplementary Table S6), or *Dynlt1* in vertebrates, has been found to play a key role in neurite outgrowth in vertebrates (Chuang et al. 2005; Sachdev et al. 2007) among other functions. *Snap25* (#47 in Supplementary Table S6) functions in both axon growth and neurotransmitter release (Osen-Sand et al. 1993; Hodel 1998). In addition, *Ppp1r9a* (# 223), located in the CI of QTL1.5f, also functions in neurite formation (Nakanishi et al. 1997).

We also identified two candidate genes involved in pacemaking or central pattern generator functioning. First, the calcium activated chloride channel, coded by *Ano1* (#116 in Supplementary Table S6), participates in the pacemaker for rhythmic slow waves in intestinal cells of Cajal (ICC) and ICC-like cells in urinary and reproductive systems in mammals (Huang et al. 2009; Hwang et al. 2009; Takaki et al. 2010; Dixon et al. 2012). Interestingly, this channel is also implicated in pacemaking of spontaneous periodic activities around hearing onset in murine cochlea (Yi et al. 2013; Wang et al. 2015).

Further, in mouse, *Ano1* is strongly expressed in auditory brainstem nuclei with exclusive expression in the presynaptic endings, implicating its function in high frequency synaptic transmission of auditory signals (Cho et al. 2014). These data render *Ano1* an exciting candidate gene regulating both rhythmic muscle activities and development and signal processing in auditory systems in vertebrates. It is unclear if invertebrate homologs of *Ano1* also play a role in rhythm generation; in *Drosophila*, *Ano1* functions in pathogen defense (Wong et al. 2013) and act as a heat sensor in nociception neurons (Cho et al. 2012). Second, innexin 2 (#78 in Supplementary Table S6), located within the CIs of QTL1.5f and immediately outside QTL1.2m, is a structural component of gap junctions. This gene is important for central pattern generators in stomatogastric and cardiac ganglia by enabling functional electrical coupling of neurons in invertebrates (Güiza et al. 2018). However, it is not yet known whether innexin 2 functions in rhythm-generating networks for thoracic muscles or auditory processing.

Lastly, we have identified a homolog of the *Drosophila* calmodulin-binding transcription activator (*Camta*) on S004073, a scaffold immediately flanking the peak of QTL1.3m (# 119 in Supplementary Table S6). This gene has been found to host the *croaker* (*cro*) locus (Sato et al. 2019), implicated in interspecific variation in interpulse interval (IPI) of the pulse song between *Drosophila sechellia* and *Drosophila simulans* (Gleason and Ritchie 2004). Mutants of *cro* have polycyclic pulse songs and prolonged IPI in *D. melanogaster* (Yokokura et al. 1995). The causal role of this gene in song rhythm regulation in another insect that also produce songs with wings renders it a strong candidate for pulse rate variation in *Laupala*.

In sum, our fine mapping provides exceptionally strong support for a type I genetic architecture underlying the species difference in pulse rate and preference, suggesting that the evolutionary process leading to a behavioral barrier consists of accumulation of small phenotypic differences in *Laupala*. During this process, genetic coupling between male and female traits may have contributed to the rapid speciation between the parental species. Our annotation of the relevant genomic region, made possible by improved mapping resolution and precision and use of sequence-based SNP markers, revealed numerous intriguing candidate genes, providing logical targets for future functional tests.

Supplementary Material

Supplementary material can be found at *Journal of Heredity* online.

Funding

National Science Foundation (1257682 to K.L.S).

Acknowledgments

We thank Ben Weaver, Alex Thomas, Eric Cole, Laura Hernandez, Isabelle Phillipe, Nathan Barr, and McKenzie Laws for assistance in cricket rearing and phenotyping, Cornell Genomic Diversity Facility for advice on molecular procedures, and Aure Bombarely, Thomas Blankers, Karl Broman, Sara Miller, Linlin Zhang, and Cornell BioHPC lab for advice and discussions on bioinformatics and QTL mapping.

Author Contributions

K.L.S. and M.X. designed research, K.L.S. collected male phenotypic data, M.X. collected female phenotypic and genomic data, M.X. conducted data analysis, and M.X. and K.L.S. wrote the article.

Data Accessibility

DNA sequences are available at NCBI (accession PRJNA628985). Phenotype and genotype data as well as bioinformatic and QTL mapping scripts can be downloaded at https://github.com/MingziXu/QTL1_fine_mapping.

References

Alexander RD. 1962. Evolutionary change in cricket acoustical communication. *Evolution*. 16:443–467.

Apweiler R, Bairoch A, Wu CH, Barker WC, Boeckmann B, Ferro S, Gasteiger E, Huang H, Lopez R, Magrane M, *et al.* 2004. UniProt: the Universal Protein knowledgebase. *Nucleic Acids Res*. 32:D115–D119.

Aronesty E. 2011. *ea-utils: command-line tools for processing biological sequencing data*. Durham (NC): Expression Analysis.

Ashburner M, Ball CA, Blake JA, Botstein D, Butler H, Cherry JM, Davis AP, Dolinski K, Dwight SS, Eppig JT. 2000. Gene ontology: tool for the unification of biology. *Nat Genet*. 25:25.

Bailey NW, Veltsos P, Tan YF, Millar AH, Ritchie MG, Simmons LW. 2013. Tissue-specific transcriptomics in the field cricket *Teleogryllus oceanicus*. *G3 (Bethesda)*. 3:225–230.

Bay RA, Arnegard ME, Conte GL, Best J, Bedford NL, McCann SR, Dubin ME, Chan YF, Jones FC, Kingsley DM, *et al.* 2017. Genetic coupling of female mate choice with polygenic ecological divergence facilitates stickleback speciation. *Curr Biol*. 27:3344–3349.e4.

Berdan EL, Blankers T, Waurick I, Mazzoni CJ, Mayer F. 2016. A genes eye view of ontogeny: de novo assembly and profiling of the *Gryllus rubens* transcriptome. *Mol Ecol Resour*. 16:1478–1490.

Blankers T, Oh KP, Bombarely A, Shaw KL. 2018. The genomic architecture of a rapid island radiation: recombination rate variation, chromosome structure, and genome assembly of the Hawaiian Cricket Laupala. *Genetics*. 209:1329–1344.

Blankers T, Oh KP, Shaw KL. 2018. The genetics of a behavioral speciation phenotype in an island system. *Genes*. 9:346.

Blankers T, Oh KP, Shaw KL. 2019. Parallel genomic architecture underlies repeated sexual signal divergence in Hawaiian *Laupala* crickets. *P Roy Soc B*. 286:20191479.

Brand P, Hinojosa-Díaz IA, Ayala R, Daigle M, Obiols CLY, Eltz T, Ramírez SR. 2019. An olfactory receptor gene underlies reproductive isolation in perfume-collecting orchid bees. *bioRxiv*.537423.

Broman KW, Wu H, Sen S, Churchill GA. 2003. R/qtl: QTL mapping in experimental crosses. *Bioinformatics*. 19:889–890.

Butlin R, Ritchie M. 1989. Genetic coupling in mate recognition systems: what is the evidence? *Biol J Linn Soc*. 37:237–246.

Cantarel BL, Korf I, Robb SM, Parra G, Ross E, Moore B, Yandell M. 2008. MAKER: an easy-to-use annotation pipeline designed for emerging model organism genomes. *Genome Res*. 18:188–196.

Chagnaud BP, Bass AH. 2014. Vocal behavior and vocal central pattern generator organization diverge among toadfishes. *Brain Behav Evol*. 84:51–65.

Cho SJ, Jeon JH, Yeo SW, Kim I-B. 2014. Anoctamin 1 expression in the mouse auditory brainstem. *Cell Tissue Res*. 357:563–569.

Cho H, Yang YD, Lee J, Lee B, Kim T, Jang Y, Back SK, Na HS, Harfe BD, Wang F, *et al.* 2012. The calcium-activated chloride channel anoctamin 1 acts as a heat sensor in nociceptive neurons. *Nat Neurosci*. 15:1015–1021.

Chuang JZ, Yeh TY, Bollati F, Conde C, Canavosio F, Caceres A, Sung CH. 2005. The dynein light chain Tctex-1 has a dynein-independent role in actin remodeling during neurite outgrowth. *Dev Cell*. 9:75–86.

Coyne JA, Orr HA. 2004. *Speciation*. Sunderland (MA): Sinauer.

Danecek P, Auton A, Abecasis G, Albers CA, Banks E, DePristo MA, McVean G. 2011. The variant call format and VCFtools. *Bioinformatics*. 27:2156–2158.

Danley PD, DeCarvalho TN, Fergus DJ, Shaw KL. 2007. Reproductive asynchrony and the divergence of Hawaiian crickets. *Ethology*. 113:1125–1132.

Ding Y, Berrocal A, Morita T, Longden KD, Stern DL. 2016. Natural courtship song variation caused by an intronic retroelement in an ion channel gene. *Nature*. 536:329–332.

Dixon RE, Hennig GW, Baker SA, Britton FC, Harfe BD, Rock JR, Sanders KM, Ward SM. 2012. Electrical slow waves in the mouse oviduct are dependent upon a calcium activated chloride conductance encoded by Tmem16a. *Biol Reprod*. 86:1–7.

Ellison CK, Shaw KL. 2013. Additive genetic architecture underlying a rapidly evolving sexual signaling phenotype in the Hawaiian cricket genus Laupala. *Behav Genet*. 43:445–454.

Elshire RJ, Glaubitz JC, Sun Q, Poland JA, Kawamoto K, Buckler ES, Mitchell SE. 2011. A robust, simple genotyping-by-sequencing (GBS) approach for high diversity species. *PLoS One*. 6:e19379.

Fang S, Takahashi A, Wu CI. 2002. A mutation in the promoter of desaturase 2 is correlated with sexual isolation between Drosophila behavioral races. *Genetics*. 162:781–784.

Fisher RA. 1930. *The genetical theory of natural selection: a complete variorum edition*. Oxford (UK): Oxford University Press.

Fowler-Finn KD, Rodríguez RL. 2016. The causes of variation in the presence of genetic covariance between sexual traits and preferences. *Biol Rev*. 91:498–510.

Garrison E. 2012. *Vcflib: A C++ library for parsing and manipulating VCF files*. GitHub: https://github.com/ekg/vcflib

Garrison E, Marth G. 2012. Haplotype-based variant detection from short-read sequencing. *arXiv preprint arXiv*.1207.3907.

Gleason JM, Ritchie MG. 2004. Do quantitative trait loci (QTL) for a courtship song difference between Drosophila simulans and D. sechellia coincide with candidate genes and intraspecific QTL? *Genetics*. 166:1303–1311.

Gould F, Estock M, Hillier NK, Powell B, Groot AT, Ward CM, Emerson JL, Schal C, Vickers NJ. 2010. Sexual isolation of male moths explained by a single pheromone response QTL containing four receptor genes. *Proc Natl Acad Sci U S A*. 107:8660–8665.

Güiza J, Barria I, Saez JC, Vega JL. 2018. Innexins: expression, regulation and functions. *Front Physiol*. 9:1414.

Harris-Warrick RM. 2010. General principles of rhythmogenesis in central pattern generator networks. *Prog Brain Res*. 187:213–222. Elsevier.

Henry CS, Martínez Wells ML, Holsinger KE. 2002. The inheritance of mating songs in two cryptic, sibling lacewing species (Neuroptera: Chrysopidae: Chrysoperla). *Genetica*. 116:269–289.

Hodel A. 1998. SNAP-25. *Int J Biochem Cell Biol*. 30:1069–1073.

Huang F, Rock JR, Harfe BD, Cheng T, Huang X, Jan YN, Jan LY. 2009. Studies on expression and function of the TMEM16A calcium-activated chloride channel. *Proc Natl Acad Sci U S A*. 106:21413–21418.

Hwang SJ, Blair PJA, Britton FC, O'Driscoll KE, Hennig G, Bayguinov YR, Rock JR, Harfe BD, Sanders KM, Ward SM. 2009. Expression of anoctamin 1/TMEM16A by interstitial cells of Cajal is fundamental for slow wave activity in gastrointestinal muscles. *J Physiol*. 587:4887–4904.

Katz PS. 2016. Evolution of central pattern generators and rhythmic behaviours. *Philos Trans R Soc Lond B Biol Sci*. 371:20150057.

Kopp M, Servedio MR, Mendelson TC, Safran RJ, Rodríguez RL, Hauber ME, Scordato EC, Symes LB, Balakrishnan CN, Zonana DM, *et al*. 2018. Mechanisms of assortative mating in speciation with gene flow: connecting theory and empirical research. *Am Nat*. 191:1–20.

Korf I. 2004. Gene finding in novel genomes. *BMC Bioinformatics*. 5:59.

Kronforst MR, Young LG, Kapan DD, McNeely C, O'Neill RJ, Gilbert LE. 2006. Linkage of butterfly mate preference and wing color preference cue at the genomic location of wingless. *Proc Natl Acad Sci U S A*. 103:6575–6580.

Lande R. 1981. Models of speciation by sexual selection on polygenic traits. *Proc Natl Acad Sci U S A*. 78:3721–3725.

Lande R. 1984. The genetic correlation between characters maintained by selection, linkage and inbreeding. *Genetics Res*. 44:309–320.

Langmead B, Salzberg SL. 2012. Fast gapped-read alignment with Bowtie 2. *Nat Methods*. 9:357–359.

Limousin D, Streiff R, Courtois B, Dupuy V, Alem S, Greenfield MD. 2012. Genetic architecture of sexual selection: QTL mapping of male song and female receiver traits in an acoustic moth. *PLoS One*. 7:e44554.

Mendelson TC, Shaw KL. 2002. Genetic and behavioral components of the cryptic species boundary between Laupala cerasina and *L. kohalensis* (Orthoptera: Gryllidae). *Genetica*. 116:301–310.

Mendelson TC, Shaw KL. 2005. Sexual behaviour: rapid speciation in an arthropod. *Nature*. 433:375–376.

Merrill RM, Rastas P, Martin SH, Melo MC, Barker S, Davey J, McMillan WO, Jiggins CD. 2019. Genetic dissection of assortative mating behavior. *PLoS Biol*. 17:e2005902.

Nakanishi H, Obaishi H, Satoh A, Wada M, Mandai K, Satoh K, Nishioka H, Matsuura Y, Mizoguchi A, Takai Y. 1997. Neurabin: a novel neural tissue–specific actin filament–binding protein involved in neurite formation. *J Cell Biol*. 139:951–961.

Oh KP, Fergus DJ, Grace JL, Shaw KL. 2012. Interspecific genetics of speciation phenotypes: song and preference coevolution in Hawaiian crickets. *J Evol Biol*. 25:1500–1512.

Oh KP, Shaw KL. 2013. Multivariate sexual selection in a rapidly evolving speciation phenotype. *Proc R Soc Lond B*. 280:20130482.

Osen-Sand A, Catsicas M, Staple JK, Jones KA, Ayala G, Knowles J, Grenningloh G, Catsicas S. 1993. Inhibition of axonal growth by SNAP-25 antisense oligonucleotides in vitro and in vivo. *Nature*. 364:445–448.

Otte D. 1994. *The crickets of Hawaii: origin, systematics and evolution*. Philadelphia (PA): The Orthopterists' Society, Academy of National Science of Philadelphia.

Panhuis TM, Butlin R, Zuk M, Tregenza T. 2001. Sexual selection and speciation. *Trends Ecol Evol*. 16:364–371.

Pascoal S, Cezard T, Eik-Nes A, Gharbi K, Majewska J, Payne E, Ritchie MG, Zuk M, Bailey NW. 2014. Rapid convergent evolution in wild crickets. *Curr Biol*. 24:1369–1374.

Reed RD, Papa R, Martin A, Hines HM, Counterman BA, Pardo-Diaz C, Jiggins CD, Chamberlain NL, Kronforst MR, Chen R, *et al*. 2011. optix drives the repeated convergent evolution of butterfly wing pattern mimicry. *Science*. 333:1137–1141.

Ritchie MG. 2007. Sexual selection and speciation. *Annu Rev Ecol Syst*. 38:79–102.

Roff DA, Fairbairn DJ. 2014. The evolution of phenotypes and genetic parameters under preferential mating. *Ecol Evol*. 4:2759–2776.

Sachdev P, Menon S, Kastner DB, Chuang J-Z, Yeh T-Y, Conde C, Caceres A, Sung C-H, Sakmar TP. 2007. G protein βγ subunit interaction with the dynein light-chain component Tctex-1 regulates neurite outgrowth. *EMBO J*. 26:2621–2632.

Saldamando CI, Miyaguchi S, Tatsuta H, Kishino H, Bridle JR, Butlin RK. 2005. Inheritance of song and stridulatory peg number divergence between *Chorthippus brunneus* and *C. jacobsi*, two naturally hybridizing grasshopper species (Orthoptera: Acrididae). *J Evol Biol*. 18:703–712.

Sato K, Ahsan MT, Ote M, Koganezawa M, Yamamoto D. 2019. Calmodulin-binding transcription factor shapes the male courtship song in Drosophila. *PLoS Genet*. 15:e1008309.

Schöneich S, Hedwig B. 2017. Neurons and Networks Underlying Singing Behaviour. In: Horch HW, Mito T, Popadić A, Ohuchi H, Noji S, editors. *The cricket as a model organism*. Tokyo (Japan): Springer. p. 141–153.

Schöneich S, Kostarakos K, Hedwig B. 2015. An auditory feature detection circuit for sound pattern recognition. *Sci Adv*. 1:e1500325.

Shaw KL. 2000. Interspecific genetics of mate recognition: inheritance of female acoustic preference in Hawaiian crickets. *Evolution*. 54:1303–1312.

Shaw KL, Herlihy DP. 2000. Acoustic preference functions and song variability in the Hawaiian cricket Laupala cerasina. *Proc Biol Sci*. 267:577–584.

Shaw KL, Lesnick SC. 2009. Genomic linkage of male song and female acoustic preference QTL underlying a rapid species radiation. *Proc Natl Acad Sci U S A*. 106:9737–9742.

Shaw KL, Mullen SP. 2011. Genes versus phenotypes in the study of speciation. *Genetica*. 139:649–661.

Shaw KL, Parsons YM, Lesnick SC. 2007. QTL analysis of a rapidly evolving speciation phenotype in the Hawaiian cricket Laupala. *Mol Ecol*. 16:2879–2892.

Singh ND, Shaw KL. 2012. On the scent of pleiotropy. *Proc Natl Acad Sci U S A*. 109:5–6.

Slater GS, Birney E. 2005. Automated generation of heuristics for biological sequence comparison. *BMC Bioinformatics*. 6:31.

Stanke M, Morgenstern B. 2005. AUGUSTUS: a web server for gene prediction in eukaryotes that allows user-defined constraints. *Nucleic Acids Res*. 33:W465–W467.

Takaki M, Suzuki H, Nakayama S. 2010. Recent advances in studies of spontaneous activity in smooth muscle: ubiquitous pacemaker cells. *Prog Biophys Mol Biol*. 102:129–135.

Templeton AR. 1981. Mechanisms of speciation-a population genetic approach. *Annu Rev Ecol Syst*. 12:23–48.

Tosches MA. 2017. Developmental and genetic mechanisms of neural circuit evolution. *Dev Biol*. 431:16–25.

Uy JAC, Irwin DE, Webster MS. 2018. Behavioral isolation and incipient speciation in birds. *Annu Rev Ecol Evol Syst*. 49:1–24.

Van Ooijen JW. 2006. *JoinMap® 4, software for the calculation of genetic linkage maps in experimental populations*. Wageningen: Kyazma BV. 33.

Wang HC, Lin CC, Cheung R, Zhang-Hooks Y, Agarwal A, Ellis-Davies G, Rock J, Bergles DE. 2015. Spontaneous activity of cochlear hair cells triggered by fluid secretion mechanism in adjacent support cells. *Cell*. 163:1348–1359.

Wiley C, Ellison CK, Shaw KL. 2012. Widespread genetic linkage of mating signals and preferences in the Hawaiian cricket Laupala. *Proc Biol Sci*. 279:1203–1209.

Wiley C, Shaw KL. 2010. Multiple genetic linkages between female preference and male signal in rapidly speciating Hawaiian crickets. *Evolution*. 64:2238–2245.

Wilkinson GS, Breden F, Mank JE, Ritchie MG, Higginson AD, Radwan J, Jaquiery J, Salzburger W, Arriero E, Barribeau SM, *et al*. 2015. The locus of sexual selection: moving sexual selection studies into the post-genomics era. *J Evol Biol*. 28:739–755.

Wong XM, Younger S, Peters CJ, Jan YN, Jan LY. 2013. Subdued, a TMEM16 family Ca^{2+}-activated Cl^-channel in Drosophila melanogaster with an unexpected role in host defense. *Elife*. 2:e00862.

Xu M, Shaw KL. 2019a. Genetic coupling of signal and preference facilitates sexual isolation during rapid speciation. *Proc Biol Sci*. 286:20191607.

Xu M, Shaw KL. 2019b. The genetics of mating song evolution underlying rapid speciation: linking quantitative variation to candidate genes for behavioral isolation. *Genetics*. 211:1089–1104.

Xu M, Shaw KL. 2020. Spatial mixing between calling males of two closely related, sympatric crickets suggests beneficial heterospecific interactions in a nonadaptive radiation. *J Hered*. 111:84–91.

Yi E, Lee J, Lee CJ. 2013. Developmental role of anoctamin-1/TMEM16A in Ca2+-dependent volume change in supporting cells of the mouse Cochlea. *Experimental neurobiology*. 22:322–329.

Yokokura T, Ueda R, Yamamoto D. 1995. Phenotypic and molecular characterization of croaker, a new mating behavior mutant of *Drosophila melanogaster*. *The Japanese Journal of Genetics*. 70:103–117.

Zeng V, Ewen-Campen B, Horch HW, Roth S, Mito T, Extavour CG. 2013. Developmental gene discovery in a hemimetabolous insect: de novo assembly and annotation of a transcriptome for the cricket Gryllus bimaculatus. *PLoS One*. 8:e61479.